Advanced Electronic Materials

ADVANCED ELECTRONIC MATERIALS Open Access

www.advelectronicmat.de

RESEARCH ARTICLE OPEN ACCESS

Performance and Environmental Impact of Flexible Temperature Sensors on Cellulose-Based Substrate

Dianne C. Corsino[1] | Diego Ferri[1] | Claudio Bonizzoni[1,2] | Marco Affronte[1,2] | Shuvaraj Ghosh[2] | Stefania Benedetti[2] | Alberto Rota[1,3,2] | Antonio Ballestrazzi[1] | Luca Pasquali[4,5,6] | Ahmed Rasheed[7] | Luisa Petti[7] | Hafiza Faiqa Maqsood[7] | Niko Münzenrieder[7] | Roberto Rosa[8] | Giuseppe Cantarella[1,2]

[1]Department of Physics, Informatics and Mathematics, University of Modena and Reggio Emilia, Modena, Italy | [2]Istituto Nanoscienze – CNR, Modena, Italy | [3]Centro Interdipartimentale INTERMECH-MO.RE., University of Modena and Reggio Emilia, Modena, Italy | [4]"Enzo Ferrari" Department of Engineering, University of Modena and Reggio Emilia, Modena, Italy | [5]CNR – Istituto Officina dei Materiali (IOM), Trieste, Italy | [6]Department of Physics, University of Johannesburg, Auckland Park, South Africa | [7]Faculty of Engineering, Free University of Bozen-Bolzano, Bozen-Bolzano, Italy | [8]Department of Science and Methods for Engineering, University of Modena and Reggio Emilia, Reggio Emilia, Italy

Correspondence: Dianne C. Corsino (dianne.corsino@unimore.it) | Giuseppe Cantarella (giuseppe.cantarella@unimore.it)

Received: 31 March 2026 | **Revised:** 30 May 2026 | **Accepted:** 15 July 2026

Keywords: circular electronics | life cycle assessment | nature-derived substrate | recoverable substrate | temperature sensors

ABSTRACT

To tackle the alarming generation of electronic waste, sustainable strategies must not be presented blindly without quantitatively assessing their environmental impacts. Here, a nature-based flexible substrate called Triacetyl Cellulose (TAC) is analyzed as an eco-friendly alternative to the widely-used polyimide, not only by demonstrating functional thin-film sensors but also through substrate recovery and reusability, and evaluation of associated environmental benefits through a life cycle assessment (LCA). Resistance temperature detectors (RTDs) and thermistors are realized on the TAC substrate using Cu, Mo, and AZO contacts, and InGaZnO. The temperature response of Cu- and Mo-based RTDs show negligible hysteresis over multiple thermal cycles, while the AZO-based RTD and the thermistors show consistent resistance drift. The sensors' mechanical performance is evaluated by bending measurements involving radii down to 2.5 mm. We further show TAC recovery by Mo RTD dissolution in deionized water and TAC reusability by another sensor fabrication. Finally, LCA is employed to reliably compare the potential environmental implications of utilizing TAC in comparison with polyimide. Key results show that sensor fabrication on TAC demonstrates lower relative impacts than polyimide in all impact categories, including resource use and climate change, making it a more sustainable substrate choice for the fabrication of thin-film temperature sensors.

1 | Introduction

Thin-film electronics have become foundational components across diverse sectors such as consumer electronics, industrial manufacturing, agriculture, and medicine, reshaping modern technological paradigms. However, their extensive utilization has long posed challenges on sustainability. The rapid turnover of devices facilitating accelerated technological advancement results in the generation of electronic waste. Every year, a production of about 62 million tons of electronic waste is reported, which is enough to fill 1.5 million transport trucks [1]. In addition to e-waste management, further hurdles need to be addressed, such as recycling scarce materials, minimizing energy requirements during electronics production, and selecting non-toxic materials and solvents [2].

A popular approach to alleviating the problem of electronic waste is the construction of electronic devices using non-toxic

materials that can be either broken down into harmless and smaller by-products or extracted for reusability [3]. Generally, the major contributor to the total volume of thin-film electronics is the substrate, which serves as the primary structural platform. That is, utilizing a flexible substrate enables the fabrication of devices with high mechanical adaptability, thereby enabling a wider range of versatile applications such as flexible and rollable displays [4], wearables and smart textiles [5, 6], and skin-like biosensors and implantable devices [7, 8]. Polymer-based films, such as polyimide (PI) [9–11], polyethylene terephthalate (PET) [11–13], and polyethylene naphthalate (PEN) [11, 12, 14], are the most prevalent carriers for flexible electronics due to their favorable mechanical properties and processability. Despite their ubiquity, the reliance on petroleum-derived plastics presents significant environmental challenges, starting from carbon-intensive manufacturing processes to the persistent issue of non-biodegradable electronic waste. The synthesis of these foils often requires harsh and toxic organic solvents and high thermal budgets [15–17], which contribute to a substantial carbon footprint before the device even reaches its use phase.

To mitigate these impacts, recent research directions pivoted toward green electronics, exploring sustainable alternatives to plastic substrates such as nanocellulose [18, 19], shellac [20], and biocomposites derived from food waste such as fruits and vegetables [21, 22]. These materials offer a unique combination of intrinsic biodegradability and tunable mechanical properties, providing a sustainable pathway for the next generation of eco-friendly, high-performance flexible devices. In particular, cellulose, being an ingredient abundant in nature, has been an attractive material for sustainable electronics. Cellulose nanofibril (CNF) papers have been particularly promising because they combine good surface flatness (i.e., low surface roughness), transparency, and mechanical robustness, and further demonstrated fungal/soil biodegradation. High-performance flexible devices including radio frequency (RF) and digital components have been fabricated directly on CNF [23]. Meanwhile, CNF nanocomposites with hydroxyethyl cellulose show improved printability and dimensional stability for printed electronics [24]. In terms of balancing mechanical properties and sensing performance, regenerated cellulose from agricultural waste has shown promise by regulating hydrogen-bonding networks [25]. Triacetylcellulose (TAC) film is another derivative that has previously been shown to be suitable for thin-film deposition and fabrication of temperature sensors, transistors and circuits [26]. Its commercial availability makes it possible to work with consistent substrate characteristics for various device fabrication processes, and at the same time, define specific physical and chemical properties as they can be tailored for technical, wearable, and medical applications. Alternatively, protein-based materials, especially silk fibroin, offer biocompatible substrates, dielectrics, and encapsulants with tunable dissolution kinetics through crystallinity control, highlighting their role in soft, biodegradable wearables and biointerfaces [27].

Although there are a growing number of solutions to mitigating the environmental impact of conventional device design and fabrication, it is equally important to quantify the sustainability that these proposed means claim. Analyzing the environmental impact of a technology through a systematic life cycle assessment (LCA) is a useful method that started to gain popularity in the community [28, 29]. By conducting an LCA, it enables a reliable comparison of different processes and products in terms of the subject of sustainability. In general, the life cycle of a product can be divided into three phases, namely the fabrication phase, the use phase, and the end-of-life phase. LCA does not need to cover the complete life cycle of a product but can focus only on defined scenarios that cover one or two of these phases and explicitly define the boundaries of the system studied.

In this work, we report the use of a flexible and commercially-available cellulose-based film, called Triacetyl Cellulose (TAC), to fabricate temperature sensors, to demonstrate substrate recovery and reusability, and to critically analyze its environmental implications compared to the widely used flexible polyimide substrate. Resistance temperature detectors (RTDs) are realized using various contacts, namely copper (Cu), molybdenum (Mo) as a biodegradable and biocompatible metal, and transparent aluminum-doped zinc oxide (AZO). Thermistors are obtained with a layer made of an indium-gallium-zinc-oxide (IGZO) semiconductor on top of the mentioned contacts. We show minimal hysteresis in the temperature response of Cu- and Mo-based RTDs consistent over five heating and cooling cycles within a period of up to 17 h, together with their characteristic positive temperature coefficient. A resistance drift throughout multiple thermal cycles, on the other hand, is noticeably present for the AZO-based RTD and the thermistors accompanied by a negative temperature coefficient. The metal-based sensors further show full functionality down to a bending radius of 5 mm, while those containing AZO become significantly resistive once bent to a bending radius of 10 mm, reaching a resistance value of more than 30 times higher than the initial value obtained in flat condition, that is, equivalent to irrecoverably high resistance of up to hundreds of megaohm. The TAC substrate recovery was performed by dissolving a Mo-based RTD in deionized water and its reusability was validated by demonstrating new functional sensors. Finally, with the goal to proactively present a quantitative and trustworthy sustainability assessment, we performed a LCA for a functional unit defined as a set of Mo-based RTDs realized on either the commonly-used polyimide or the nature-based TAC substrate. Key results of the LCA reveal chemical use and waste treatment as the main contributors to the environmental impact of device fabrication on both TAC and polyimide. Comparing the two substrates, the results show lower relative impacts with the use of the TAC substrate in all impact categories with a single score equivalent to 26.4×10^{-6} Pt while that of polyimide equals 45.1×10^{-6} Pt.

2 | Results and Discussion

The properties of the TAC film are investigated and presented in Figure 1a,b. The details of the characterization performed can be found in the **Experimental Section**. Based on the transmittance measurement performed, the 38 μm-thick TAC film shows a transmittance of 35% extracted at a wavelength of 550 nm. To ensure suitability for thin-film deposition, the surface roughness of the film is assessed by Atomic Force Microscopy. Figure 1b shows a 3D surface profile of a 5 μm × 5 μm area of the TAC substrate where a mean surface roughness of 1.9 nm was obtained. Representative RTDs and thermistors fabricated on the TAC substrate as well as the schematic diagrams are illustrated

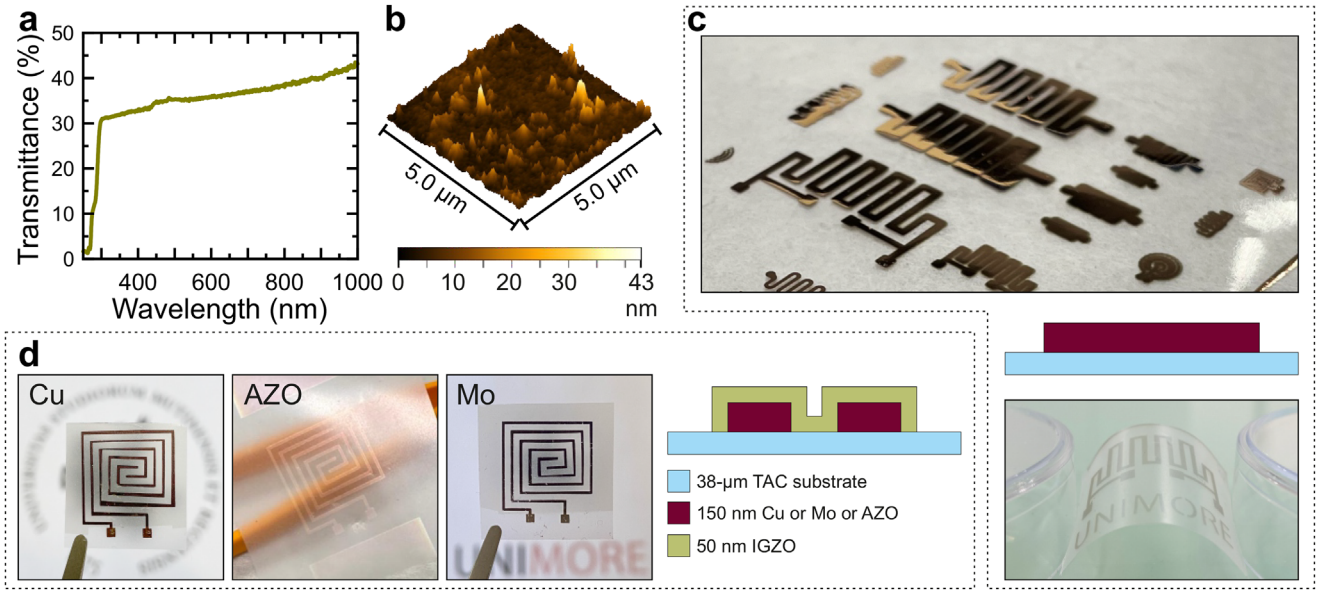

FIGURE 1 | Temperature sensor fabrication on a self-standing 38 µm-thick TAC film. (a) Transmittance spectrum and (b) 3D surface profile of a 5 µm × 5 µm area of the TAC film acquired from atomic force microscopy. Representative RTDs (c) and thermistors (d) fabricated on the TAC substrate, with the schematic diagram of the simplified device cross-section.

in Figure 1c,d, clearly showing the translucent property of the TAC film.

2.1 | Temperature Response

Two different types of temperature sensors, namely RTDs and thermistors, are realized on top of the self-standing TAC film. The RTDs are serpentine structures made with a 150 nm-thick layer of sputtered Cu, Mo, or Al:ZnO (AZO) (insets of Figure 2a-I, b-I, and c-I, respectively). The first electrical characterization of the RTDs followed a real-time resistance measurement as the temperature is swept from 35°C to 115°C and vice versa, identified as the heating and cooling half-cycles, respectively, with an interval of 10°C and a hold time of 10 min. Here, a maximum temperature of 115°C is chosen to make sure that the TAC film remains intact based on the provided glass transition temperature of 175°C and decomposition temperature of 300°C. From this measurement, the Temperature Coefficient of Resistance (TCR) or, simply, sensitivity α of the sensors can be calculated using the equation $\alpha = \frac{R-R_0}{R_0(T-T_0)}$ where R_0 is the resistance at reference temperature T_0 (here, T_0=35°C) and R is the resistance at temperature T. By plotting the relative change in resistance $\Delta R/R_0$ versus temperature, the slope of the linear fitting directly provides the sensitivity of the sensor. Cycling stability measurement, on the other hand, was conducted through a real-time resistance measurement during five heating-cooling cycles for temperatures ranging between 35°C and 95°C with an interval of 20°C and a hold time of 10 min (Figure 2a-II, III, b-II, III, and c-II, III). The response and recovery times of the sensors are calculated from the heating interval between 35°C and 55°C and cooling interval between 95°C and 75°C, respectively, of the first cycle. Here, the response and recovery times are defined as the difference between the time at 90% of the target temperature, i.e. 53°C and 77°C, and the time at which the sensor reaches 90% of its resistance at the target temperature.

The results of the single cycle measurement performed on the Cu-, Mo-, and AZO-based RTDs are shown in Figure 2a-I, b-I, and c-I wherein the average absolute resistance and relative change in resistance measured during the hold time are calculated. Here, the Cu-based and Mo-based RTDs display increasing resistance values as the temperature is increased, a behavior typical of a conductor. In particular, sweeping the temperature from 35°C to 115°C linearly increases the resistance of the Cu-based RTD from 28 to 34 Ω. Decreasing the temperature back to 35°C shows the cooling curve perfectly following the heating curve with negligible hysteresis. The calculated response and recovery times are both approximately 4 s. In particular, similar α values of 0.00264°C^{-1} and 0.0027°C^{-1} are extracted from the heating and cooling half-cycles, respectively. Note that while the resistance window is short, the Cu-based RTD demonstrated high stability within this temperature range. The reliability of Cu RTDs fabricated on the TAC substrate is further exemplified by two other sensors (Figure S1), which show similar $\Delta R/R_0$ within the same temperature window and comparable sensitivity values (0.00266°C^{-1} and 0.00272°C^{-1}, and 0.00272°C^{-1} and 0.00282°C^{-1}). This is also demonstrated in the results of the cycling measurement performed, where the electrical behavior of the Cu-based RTD displays repeatability over the five cycles, equivalent to more than 16 h of continuous operation, as shown in Figure 2a-II. The summary of $\Delta R/R_0$ obtained at specific temperatures over the five cycles classified between heating and cooling cycles is in Figure 2a-III. Here, it can be observed that, regardless of the direction of the temperature sweep, the $\Delta R/R_0$ value remains consistent over the five cycles signifying the reliability of the sensor.

In the case of Mo-based RTD (Figure 2b-I–III), increasing and decreasing trends in the resistance are similarly observed over the heating and cooling half-cycles, respectively. The Mo-based RTD exhibits higher resistance values between 1.75 and 2 kΩ, although a slightly lower relative resistance change than that

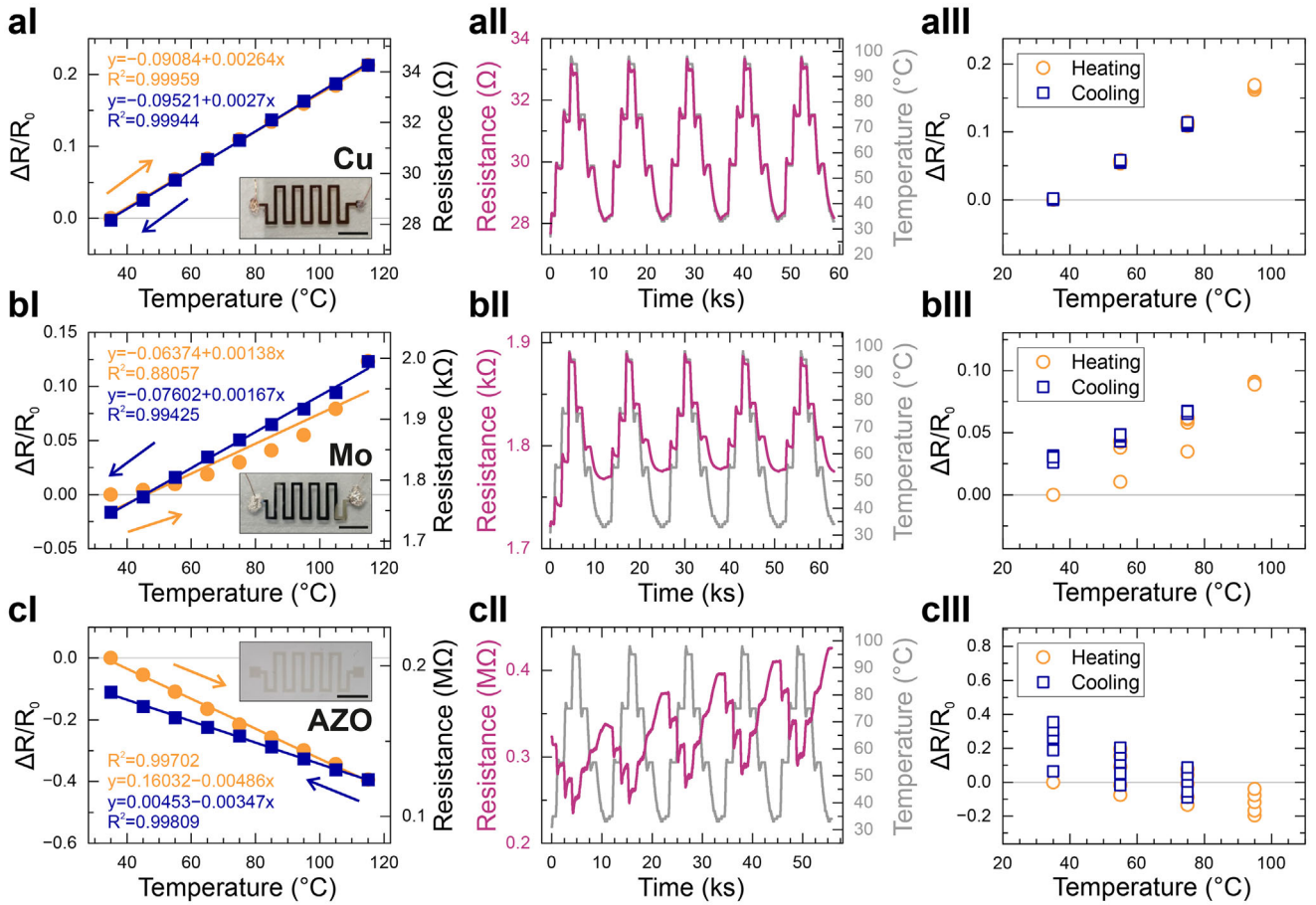

FIGURE 2 | Temperature response of the RTDs based on (a) Cu, (b) Mo, and (c) AZO fabricated on the TAC film. (I) Relative change in resistance and average resistance as a function of temperatures from 35°C to 115°C, with an interval of 10°C and hold time of 10 min (inset: images of the respective RTDs [Scale bar: 5 mm]). Solid lines represent the linear fitting used to extract the sensitivity of the sensors. (II) Resistance variation over five cycles of heating and cooling between 35°C and 95°C with an interval of 20°C and a hold time of 10 min. (III) Cluster plots of the relative resistance change obtained at defined temperatures in each heating and cooling stages over the five cycles.

of the Cu-based RTD, for the same temperature range. As can be seen in Figure 2b-I, a clear hysteresis is present whereby a drift is exhibited during the cooling half-cycle, yet a more linear relationship with temperature is achieved. This difference in linearity and the hysteresis present between the heating and cooling half-cycles are reflected on the R^2 values and α of $0.00138°C^{-1}$ and $0.00167°C^{-1}$. The observed hysteresis is also apparent in the cycling measurement results, indicating that the first heating half-cycle is needed to stabilize the temperature-dependent behavior of the Mo-based RTD. Indeed, the next four cycles present a more stable sensor performance that shows only minimal drift in the average resistance values, and thus in $\Delta R/R_0$, as can be seen in the cluster plot in Figure 2b-III. A response time of about 4 s and a recovery time of around 28 s is obtained for the Mo-based RTD. In contrast to what was observed for Cu- and Mo-based RTD, the AZO-based RTD exhibits an inversely proportional electrical behavior with respect to temperature. A resistance decrease of almost 40% from 205 to 124 kΩ is obtained by increasing the temperature from 35°C to 115°C, which again increased to 182 kΩ, about 10% lower than the initial resistance, at the end of the cooling half-cycle. The extracted α values are $-0.00486°C^{-1}$ and $-0.00347°C^{-1}$ in the heating and cooling phases, respectively, while the response and recovery times are approximately 4 and 121 s. This negative temperature coefficient is a characteristic of an oxide material where increasing the temperature provides thermal energy to the system which in turn decreases the net resistance [30, 31]. In terms of stability, both single cycle and multiple cycling measurement display hysteresis and drift in performance as can be observed by the consistent resistance climb over the multiple thermal cycles. This could be associated to aging and/or moisture absorption that can lead to slow corrosion of the conductive path in the AZO layer.

Thermistors are made with a layer of bottom contact and a top semiconductor layer (insets of Figure 3a-I, b-I, and c-I). The three thermistors differ by the bottom contact material which is made of 150 nm-thick sputtered layer of either Cu, Mo, or AZO. All thermistors have a 50 nm-thick sputtered InGaZnO (IGZO) semiconductor film and are characterized similarly to the RTDs. The results of the single cycle and multiple cycling measurements are summarized in Figure 3 which clearly show the inverse relationship of resistance with temperature among the three thermistors. Indeed, the observed negative temperature coefficient is accounted by the presence of the IGZO semiconductor layer. Generally, we can observe higher resistance values as well as $\Delta R/R_0$ for the thermistors across the different

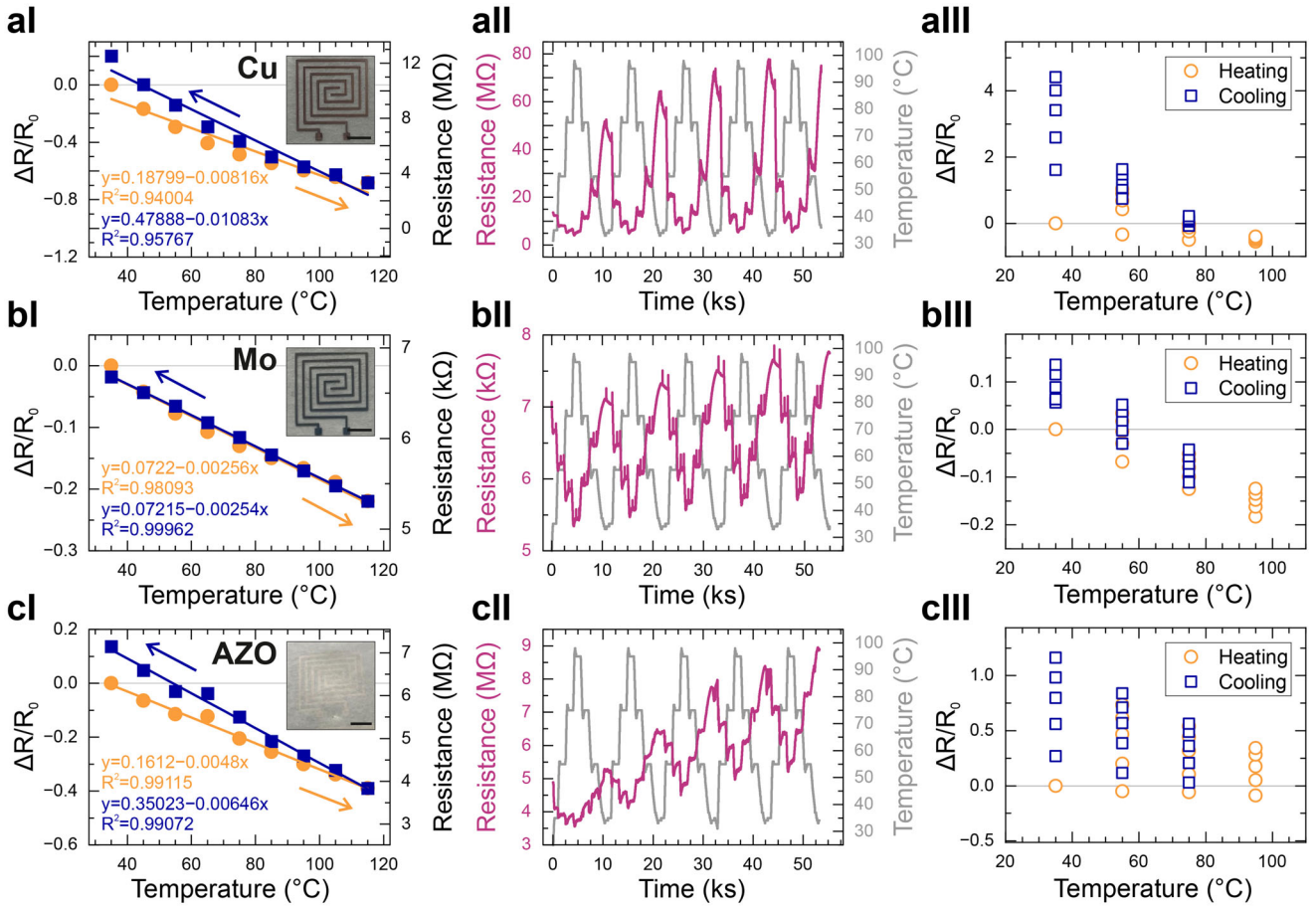

FIGURE 3 | Temperature response of the thermistors based on (a) Cu, (b) Mo, and (c) AZO, with top IGZO semiconductor layer fabricated on the TAC film. (I) Relative change in resistance and average resistance as a function of temperatures from 35°C to 115°C, with an interval of 10°C and hold time of 10 min (inset: images of the respective RTDs [Scale bar: 5 mm]). Solid lines represent the linear fitting used to extract the sensitivity of the sensors. (II) Resistance variation over five cycles of heating and cooling between 35°C and 95°C with an interval of 20°C and a hold time of 10 min. (III) Cluster plots of the relative resistance change obtained at defined temperatures in each heating and cooling stages over the five cycles.

contact materials. Based on the initial single cycle measurement illustrated in Figures 3a-I, b-I, and c-I, the measured resistance values are: (1) 3.3– 10.4 MΩ for the Cu/IGZO thermistor, (2) 5.3k – 6.8 kΩ for the Mo/IGZO thermistor, and (3) 3.8M – 7.1 MΩ for the AZO/IGZO thermistor. By linear fitting, the α values obtained in the heating and cooling cycles are (1) $-0.00816°C^{-1}$ and $-0.01083°C^{-1}$, (2) $-0.00256°C^{-1}$ and $-0.00254°C^{-1}$, and (3) $-0.0048°C^{-1}$ and $-0.00646°C^{-1}$ for Cu/IGZO, Mo/IGZO, and AZO/IGZO thermistors, respectively. Not only are hystereses present in this first cycle, but also a consistent resistance increase over the multiple thermal cycles is visible across the three types of thermistor, as also observed by other reported IGZO-based thermistors [32, 33]. At the end of the fifth cooling cycle (T = 35°C), the final resistance reached up to about 450% for the Cu/IGZO thermistor, about 14% for the Mo/IGZO thermistor, and about 120% for the AZO/IGZO thermistor of the initial measured resistance. The calculated response and recovery times are about 5 s and 5 s for Cu/IGZO, 4 s and 5 s for Mo/IGZO, and 5 and 574 s for AZO/IGZO. Overall, as exemplified by the sensor performance observed here, each type can be classified into suitable application scenarios. Owing to their accuracy and linearity, metal-based RTDs, i.e., Cu and Mo, are more appropriate for stable monitoring applications even at high temperatures such as in industrial processes. In contrast, since thermistors show a massive change in resistance over a narrow temperature window, they excel in low-to-medium temperature applications due to their high sensitivity. Moreover, since long-term drift is present in thermistors, especially when repeatedly exposed to high temperatures, high-precision monitoring is not recommended and calibration may be needed.

2.2 | Mechanical Performance

To assess the mechanical stability of the RTDs and thermistors realized on the TAC substrate, the resistance was evaluated and compared between flat, bent, and re-flat conditions. To induce bending stress, the sensors were adhered onto rods with varying radius between 2.5 and 25 mm, as represented in Figure 4a. The sequence of measurement is simplified in Figure 4b - (1) prior to inducing the bending stress, the resistance of the devices is first determined in flat condition, (2) devices are bent starting from the largest bending radius and the resistance is measured during bending, and (3) after each bending stress induced, the sensors are then re-flat to confirm functionality, or loss of it. Figure 4c–h summarizes the resistance variation observed as a function of

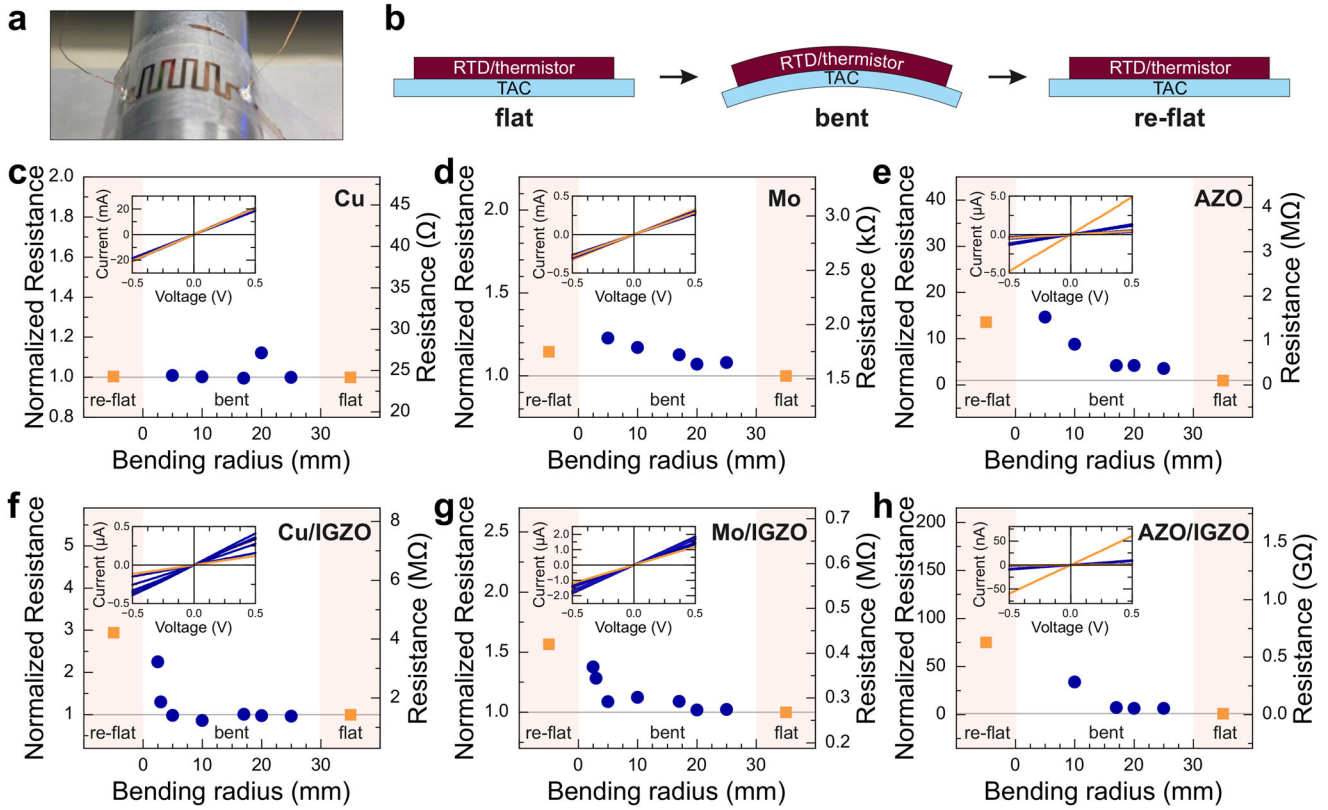

FIGURE 4 | Mechanical performance of the RTDs and thermistors fabricated on the TAC substrate. (a) Image of a representative RTD while bent on a rod of defined bending radius. (b) Measurement sequence to determine the resistance of the device against bending stress starting from a flat condition, followed by bent condition from a bending radius of 25 mm down to 2.5 mm, and finally back to a re-flat configuration. Summary of the resistance and evolution of the current-voltage plots of the (c) Cu-, (d) Mo-, and (e) AZO-based RTDs, and (f) Cu/IGZO, (g) Mo/IGZO, and (h) AZO/IGZO thermistors fabricated on the TAC film.

the bending radius and the evolution of the current-voltage plots (insets). Figure 4c shows the mechanical performance of a Cu-based RTD where a generally invariable resistance can be observed around 24 Ω, which is retained until the re-flat condition. The mechanical reliability of Cu RTD on the TAC substrate is further exemplified by other two sensors which show similar negligible resistance change to bending with radius as small as 5 mm (Figure S2). This can be attributed to the strength of both Cu and the TAC substrate (tensile strength = 80 MPa and elongation > 18%) in withstanding mechanical deformation. Similarly, the Mo-based RTD displays reliability against bending stress with only a slight increase in the resistance value from 15 to 1.9 kΩ when bent to a radius of 5 mm, as shown in Figure 4d. In a re-flat condition, the resistance goes down to 1.7 kΩ. On the other hand, the AZO-based RTD shows a significant resistance variation over the bending test as seen from Figure 4e. In a flat condition, the AZO-based RTD exhibits a resistance of 0.1 MΩ which gradually increased to 0.4 MΩ when bent down to a radius of 17 mm. A dramatic increase in the resistance can be further observed for a bending radius of 5 mm which was not substantially recovered in the re-flat condition where the resistance obtained was 1.4 MΩ, signifying almost 1500% increase. This is as expected since, as previously mentioned, the AZO is an oxide material, which is typically more brittle than the metallic conductors, making it more sensitive to bending and a possible microcrack formation [34].

The results of the bending measurements conducted for the thermistors are shown in Figure 4f–h. The Cu/IGZO thermistor exhibits a measured resistance of 1.4 MΩ in a flat condition which minimally changed until a bending radius of 5 mm. Subjecting it to smaller bending radii of 3 and 2.5 mm, however, degraded its behavior showing an increased resistance of up to 1.9 and 3.2 MΩ, respectively. The resistance of the Cu/IGZO thermistor did not recover and further degraded in the re-flat condition (4.2 MΩ). The Mo/IGZO thermistor exhibited a similarly good mechanical stability with Cu/IGZO thermistor only until a bending radius of 5 mm where the resistance changed from 268 to 292 kΩ. Smaller bending radius causes a dramatic increase in the resistance up to 369 kΩ which further increased to 420 kΩ when measured in a re-flat condition. Here, it can be said that the presence of the IGZO semiconductor made the devices less mechanically strong to withstand bending radii smaller than 5 mm. Interestingly, the AZO/IGZO thermistor exhibits inferior mechanical stability among the sensors presented here. From a value of 8.4 MΩ obtained in flat condition, this resistance already increased up to 60 MΩ at a bending radius of 17 mm. Further decreasing the bending radius to 10 mm increases its resistance to 284 MΩ which reaches more than a double of this value to 630 MΩ when measured back in a re-flat condition. The poor mechanical stability and irrecoverable electrical behavior of the AZO/IGZO thermistor are aggravated by the two semiconductor layers used in this device.

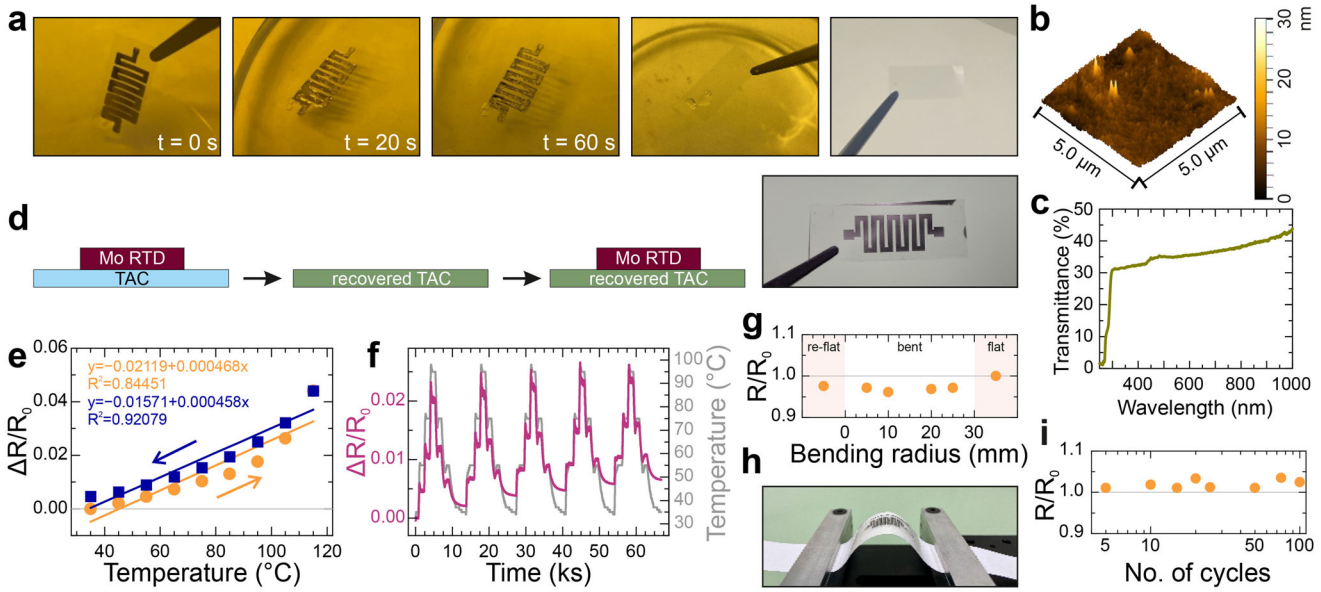

FIGURE 5 | Recovery and reusability of TAC substrate: (a) Dissolution in deionized water of Mo-based RTD fabricated on TAC substrate. (b) 3D surface profile of 5 μm × 5 μm area and (c) transmittance spectrum of the recovered TAC substrate. (d) Schematic representation of TAC substrate recovery and reusability, and an image of a representative Mo RTD fabricated on the recovered substrate. Temperature response of a Mo RTD on a recovered TAC substrate based on (e) a single temperature cycling between 35°C and 115°C and (f) multiple cycling between 35°C and 95°C. (g) Resistance variation of a Mo RTD with bending radius. (h) Image of a Mo RTD on a recovered TAC substrate bent to a radius of 10 mm in the cyclic bending setup and its resistance variation (i) up to 100 bending cycles.

2.3 | Substrate Reusability and Life Cycle Assessment

Besides employing natural raw materials for the substrate, reusability by successful recovery is another promising feature in line with circularity. A dissolution test was performed by immersing a Mo-based RTD fabricated on the TAC substrate in deionized water. Figure 5a shows the time evolution of Mo-based RTD on TAC before (t = 0 s) and during (t = 20 s and t = 60 s) immersion in water. After gently shaking the beaker, the Mo film was completely removed from the TAC substrate. This has allowed full material recovery with visually no damage from both the previous electronics fabrication and the dissolution test. To confirm the integrity of the recovered TAC substrate, its surface roughness and transparency were again assessed by AFM (Figure 5b) and transmittance analysis (Figure 5c). The results of the characterization confirm that the recovered TAC surface remains smooth and semi-transparent, exhibiting a mean surface roughness of 1.3 nm and a transparency of 35% at 550 nm, which are both comparable to the initial properties obtained from the fresh TAC substrate. To demonstrate material reusability, another RTD made of 150 nm-thick Mo was fabricated and characterized on the recovered TAC (Figure 5d). As displayed in Figure 5e,f, the temperature response to a single cycle and multiple cycling of the second generation of Mo RTD shows full functionality functionality with a sensitivity 0.000468°C^{-1} and 0.000458°C^{-1} obtained from the heating and cooling curves, respectively, and reliability over about 18 h of continuous operation. Similarly, Figure 5g illustrates that the Mo RTD exhibits minimal resistance variation under static bending down to a radius of 5 mm with a maximum deviation of only 3.9% from the initial flat condition. Furthermore, dynamic bending was performed where the Mo RTD on the recovered TAC was repeatedly subjected to a bending radius of 10 mm for up to 100 bending cycles (Figure 5h). As can be observed in Figure 5i, the resistance of the Mo RTD negligible changed where only a maximum deviation of 3.5% was obtained. These results verify the mechanical integrity of the recovered TAC for a single, and a potential multiple, reuse cycles.

The use of TAC film, which is based on an abundant natural ingredient such as cellulose, as a replacement for commonly-used non-ecofriendly plastic foils, is a starting solution to working toward sustainability in electronics fabrication. In simple context, materials made out of natural ingredients are easily labeled as sustainable, while synthetic ones are considered the opposite, disregarding the processes involved between raw material extraction and product realization. By performing a LCA on temperature sensor fabricated on the TAC substrate used in this work, a reliable comparison with the commonly-used flexible polyimide foil is obtained. As shown in Figure 6a, the functional unit chosen for this analysis was the production of a set of Mo-based RTDs on a 7.5 cm × 7.5 cm area on either a 38 μm-thick TAC substrate or on a 50 μm-thick polyimide. Other than the substrate production and Mo sputtering, the LCA also included in the system analyzed the substrate cleaning step and the end-of-life of the waste materials generated (see details in **Experimental Section**).

The environmental impacts as calculated by the EF 3.1 impact assessment method [35] at the midpoint level for the life cycle of Mo-based RTDs fabricated both on a TAC and a polyimide substrate are detailed in Table 1 and summarized in terms of relative impact percentages in Figure 6b. As clearly evident, the resistance temperature detectors prepared on the TAC substrate is characterized by lower environmental impacts with respect to the one on polyimide, independently by the impact category considered, with reduction into the environmental impacts

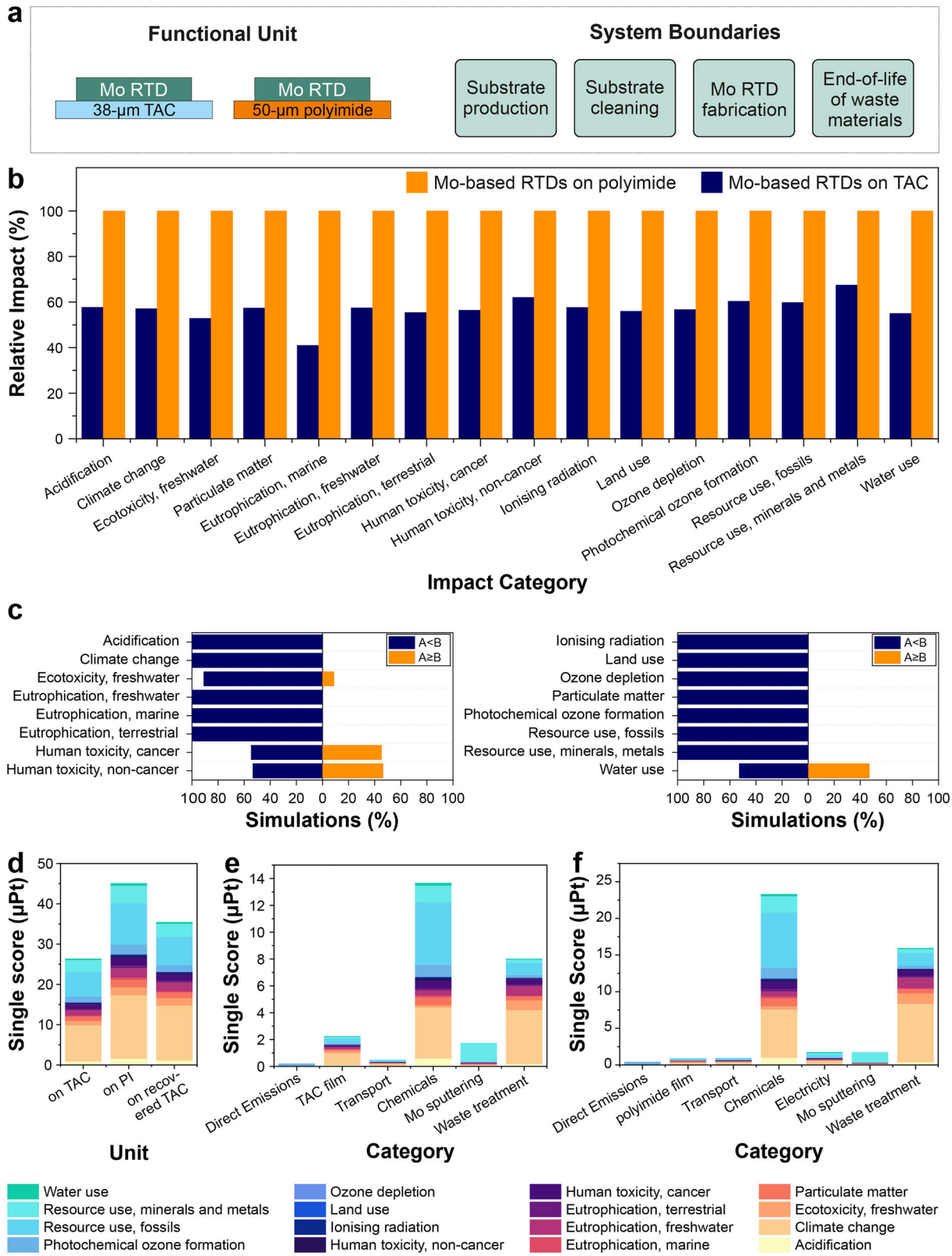

FIGURE 6 | Life cycle assessment of the fabrication of Mo RTDs on TAC substrate and polyimide film: (a) Definition of functional unit and system boundaries used in the LCA analysis. (b) Comparison of relative impact percentages in different damage categories, calculated by the EF 3.1 impact assessment method, of a set of Mo RTDs fabricated on the TAC substrate and on a commonly-used polyimide substrate. (c) Monte Carlo comparison of the two product systems A and B, showing the percentage of iterations in which A (i.e., Mo-based RTDs on TAC substrate) performs better than B, i.e., Mo-based RTDs on polyimide substrate ($A < B$) or worse/equally ($A \geq B$) across the assessed impact categories. (d) Comparison of single score expressing the potential environmental impact of the fabrication of Mo-based RTDs on a fresh TAC substrate, a polyimide film, and a recovered TAC substrate. Contributions to the single score obtained for the fabrication of a set of Mo-based RTDs on (e) TAC and (f) polyimide substrates.

TABLE 1 | Detailed midpoint results (EF 3.1 method) for the life cycle of a set of Mo-based RTD fabricated on both TAC and polyimide substrate.

Impact category	Unit	Mo-based RTDs on TAC substrate	Mo-based RTDs on polyimide substrate
Acidification	mol H^+ eq	7.94×10^{-4}	1.37×10^{-3}
Climate change	kg CO_2 eq	3.22×10^{-1}	5.65×10^{-1}
Ecotoxicity, freshwater	CTUe	3.08	5.82
Particulate matter	disease inc.	7.25×10^{-9}	1.27×10^{-8}
Eutrophication, marine	kg N eq	1.41×10^{-4}	3.44×10^{-4}
Eutrophication, freshwater	kg P eq	7.84×10^{-5}	1.36×10^{-4}
Eutrophication, terrestrial	mol N eq	1.43×10^{-3}	2.59×10^{-3}
Human toxicity, cancer	CTUh	9.36×10^{-10}	1.66×10^{-9}
Human toxicity, non-cancer	CTUh	1.97×10^{-9}	3.17×10^{-9}
Ionising radiation	kBq U-235 eq	1.36×10^{-2}	2.37×10^{-2}
Land use	Pt	6.58×10^{-1}	1.18
Ozone depletion	kg CFC11 eq	7.52×10^{-9}	1.33×10^{-8}
Photochemical ozone formation	kg NMVOC eq	1.24×10^{-3}	2.06×10^{-3}
Resource use, fossils	MJ	4.76	7.96
Resource use, minerals and metals	kg Sb eq	2.47×10^{-6}	3.67×10^{-6}
Water use	m^3 depriv.	4.93×10^{-2}	8.97×10^{-2}

ranging from −32.5% for the category Resource use, minerals and metals up to −59% for the category Eutrophication, marine. The impacts in the category climate change equal 0.322 kg CO_2 eq. and 0.565 kg CO_2 eq. for the RTD fabricated on TAC and polyimide substrate respectively, corresponding to a reduction of ca. −43% for the TAC substrate-based RTD. In both cases the main (for 89.0% and 87.9% respectively for the RTD on TAC and polyimide substrate) cause of the impact in the climate change category is the emission into air compartment of Carbon dioxide of fossil origin. This emission is associated mainly (for 47.8% and 50.3% respectively for the RTD on TAC and polyimide substrate) to the Ecoinvent dataset "Hazardous waste, for incineration Europe without Switzerland | market for hazardous waste, for incineration | APOS, U", that has been used to model the transport and the incineration end of life of the solvents employed for the cleaning of the substrates.

With the aim to quantify the reliability of the comparison performed, in relation to the uncertainties characterizing the inventory data, the Monte Carlo (MC) analysis [36] was conducted by performing 1000 runs for each calculation with a 95% confidence interval (CI). The MC simulation results are detailed in Tables S1 and S2, for the Mo-based RTDs fabricated on TAC and polyimide substrates respectively, in terms of the absolute uncertainties, i.e., the mean, the median, the standard deviation (SD), the coefficient of variation (CV), the 2.5th percentile and the 97.5th percentile (i.e., the 2.5% and 97.5%), together with the standard error of the mean (SEM). In both MC analyses, the most robust results were observed for Climate change, Acidification, Marine eutrophication and Terrestrial eutrophication, which showed comparatively low CV and relatively narrow CI. By contrast, Ecotoxicity, Human toxicity, Ionising radiation and Water use were consistently affected by high dispersion and, in some cases, confidence intervals extending to negative values, indicating substantial uncertainty and lower reliability of these impact categories.

In order to better support the statistical significance of the calculated differences, it is possible to count the number of comparison runs in which the environmental impact of product system A (i.e., Mo-based RTDs on TAC substrate) is lower than the corresponding environmental impact of product system B (i.e., Mo-based RTDs on polyimide substrate). The results for all the impact categories are reported in Figure 6c. Overall, comparative MC analysis shows statistically robust differences for the impact categories Acidification, Climate change, freshwater, marine and terrestrial Eutrophication, Ionizing radiation, Land use, Ozone depletion, Particulate matter, Photochemical ozone formation, and Resource use (both fossils and minerals-metals). Indeed, for these indicators, the impact of the Mo-based RTD on TAC substrate (i.e., product system A) is significantly (with simulation percentages close to 100%) lower with respect to the impact of the Mo-based RTD on polyimide substrate (i.e., product system B). In contrast, the comparison is less conclusive for Ecotoxicity, freshwater and above all for Human toxicity (cancer and non-cancer) and Water use, where the overlap between the two distributions is more substantial and the share of simulations for which the impact of product system A being ≥ of the impact of product system B is not negligible. In contrast, the comparison is less conclusive for Human toxicity (cancer and non-cancer) and Water use, where the overlap between the two distributions is more substantial and the share of simulations with $A \geq B$ is not negligible.

The midpoint results previously showed in Table 1 and Figure 6b can be then normalized and weighted in order to obtain an aggre-

gated indicator of potential environmental impacts expressed as a single score in environmental points (Pt). The obtained single score results are reported in Figure 6d. The single score of the Mo-based RTDs on TAC substrate is 26.4×10^{-6} Pt, corresponding to an overall reduction of 41.5% with respect to the RTDs fabricated on polyimide, the latter being 45.1×10^{-6} Pt. The main environmental hotspots associated with the life cycle of the Mo-based RTD on TAC substrate can be clearly identified by Figure 6e. Particularly, the production of the necessary chemicals employed (i.e., isopropyl alcohol, and nitrogen) contributes ca. to 53% of the overall single score, and it is followed by the treatment of the waste generated during the manufacturing process (contributing for ca. 31%), and by the production of the TAC substrate itself (contributing for ca. 9%). In the case of the Mo-based RTD on polyimide substrate, the environmental hotspot analysis, reported in Figure 6f, shows a similar trend, with the main (for ca. 52%) contribution to the single score being the production of acetone, isopropyl alcohol and nitrogen, followed by the treatment of the produced waste (contributing for ca. 35%). On the opposite with respect to the previous case, the third for importance contribution (i.e., ca. 4%) to the single score in the case of the Mo-based RTD on polyimide substrate is represented by the production of the electric energy necessary for ultrasonication and for heating the polyimide substrate at 200°C for 24 h before Mo deposition.

For the sake of comparison Figure 6d also reports a third scenario in which the TAC substrate has been regenerated by washing away the Mo-based RTD with deionized water. Quite surprisingly this third scenario is characterized by a single score of 35.5×10^{-6} Pt, i.e., the 35.5% higher with respect to the scenario in which the TAC substrate is not recovered after its first use. The reason of this finding can be argued by considering the previously discussed environmental hotspots associated to the life cycle of the Mo-based RTD on TAC substrate. The main reason lies in the end-of-life treatment of the Mo-contaminated waste stream, since hazardous waste incineration was found to be considerably more impactful than TAC substrate production itself, thus outweighing the environmental benefit expected from reuse.

Therefore, the environmental performance of the reuse scenario is strongly affected by the balance between the number of substrate reuse cycles and the amount of washing solution generated during Mo removal. However, this result depends on the assumption that a given amount of washing solution is required for each recovery operation.

Although reusing the same washing solution during the second life cycle of the same substrate may not be technically reliable, a relevant environmental trade-off can be identified in the regeneration of multiple Mo-based RTDs using the same washing solution. If the same washing solution could be used for the concurrent washing of n substrates, the environmental impacts associated with both the production/transport of the washing solution and its end-of-life treatment would be allocated among n sets of RTDs. As a result, the impact contribution of the washing step per regenerated device would decrease with increasing n, potentially improving the environmental performance of the reuse scenario. Under this assumption, the environmental burden related to the Mo-containing washing effluent would no longer increase proportionally with the number of regenerated devices, partially compensating for the high impact observed when the washing solution is treated by incineration after a single use. For instance, by modifying the LCA model by considering the possibility to use the same amount (i.e., 75 mL) of deionized water for the concurrent cleaning of n sets of RTDs, a lower single score can be reached starting from the scenario with $n = 10$, for which the single score becomes equal to 26.3×10^{-6} Pt. Similar trade-offs could also be explored by applying the same approach to the chemicals used for TAC substrate cleaning before sputtering, as their production and end-of-life treatment were identified as relevant environmental hotspots. In addition, further improvements may be achieved by increasing the number of reuse cycles that the same TAC substrate can withstand without compromising its functional performance.

Based on these findings, it becomes crucial to evaluate the importance of each step in a fabrication protocol as some trivial steps could mean a compromise in the environmental profile of the final device. Furthermore, it should be noted that different thicknesses are compared as these substrates are based on commercial availability and standards. Therefore, it is also necessary to further investigate similar material specifications, such as thickness and density, and/or to couple these differences in terms of device and mechanical performance.

3 | Conclusion

This work presents an in-depth examination of triacetyl cellulose as an ecofriendly material choice for substrates by: (1) demonstrating functional thin-film temperature sensors (i.e., RTDs and thermistors), (2) showcasing its recovery and reusability for multiple fabrication, and (3) assessing the environmental benefits associated to its use compared to the widely-used polyimide foil. Three contact materials, namely Cu, Mo, and AZO, are investigated as RTDs while thermistors are achieved through an addition of an IGZO layer. The Cu- and Mo-based RTDs exhibit negligible hysteresis throughout five thermal cycles, confirming operational stability for about 17 h. The AZO-based RTD and the thermistors display their characteristic negative temperature coefficient albeit with notable hystereses and drift in resistance across multiple thermal cycles. This could be likely due to aging and/or deterioration in the conductive path of the semiconductor layer. As for the mechanical performance of the sensors, the Cu- and Mo-based RTD show mechanical resilience when bent to a radius as small as 5 mm while its corresponding thermistor configuration show onset of mechanical failure at a radius down to 2.5 mm. In contrast, the AZO-based RTD and thermistor display a lower threshold before mechanical failure where an approximately 15 to 33 times increase in resistance are observed at radii of 5 and 10 mm. This irrecoverable behavior could be linked to the more brittle nature of semiconductors compared to metallic conductors, making the former more sensitive to bending and microcrack formation. Finally, we present the recovery and reusability of the TAC substrate by dissolving a Mo-based RTD in deionized water and subsequently fabricating a new Mo RTD on the recovered TAC, a capability supporting circularity in electronics fabrication. A life cycle assessment is conducted to quantify and proactively compare the potential

environmental impact of fabricating temperature sensors on the TAC substrate and a commonly-used polyimide film, with a functional unit defined as Mo-based RTDs fabricated on a 7.5 cm × 7.5 cm substrate area. The key LCA findings reveal that device fabrication on TAC poses lower environmental impacts across all impact categories, with a single score of 26.4×10^{-6} Pt, corresponding to an overall reduction of 41.5% with respect to device fabrication on polyimide with 45.1×10^{-6} Pt.

4 | Experimental Section

4.1 | Substrate Characterization

A commercially-available self-standing 38 μm-thick flexible triacetyl cellulose (TAC) film (MTTF38, Island Polymer Industries GmbH) was used as a substrate for the fabrication of temperature sensors. Substrate evaluation was performed by surface roughness measurement and transmittance analysis. The surface roughness of TAC was evaluated by atomic force microscopy (Veeco Nanoscope IIIa Multimode AFM). For the transmittance evaluation, the measurements were performed in transmission mode, using a laboratory-built variable-angle spectrophotometer for absorption/reflectivity. An Ocean Optics DH-2000-BAL dual deuterium-halogen was used as source. The spectrometer was an Ocean Optics USB-4000-XR, operating via optical fibers.

4.2 | Device Fabrication

Before any device fabrication, the TAC substrate was prepared by cleaning it with isopropanol for 5 min without sonication. RTDs were made with a 150 nm-thick layer of either sputtered Cu, Mo, or aluminum-doped zinc oxide (AZO). The Cu and Mo films were deposited by DC sputtering (5Pascal) using high-purity Cu and Mo targets at a power of 50 and 100 W, respectively. The AZO film was achieved by RF sputtering (Moorfield) an AZO target (ZnO/Al_2O_3 $98/2 wt.\%$) at room temperature using an RF power of 120 W. Thermistors were fabricated with a 150 nm-thick layer of either Cu, Mo, or AZO followed by a 50 nm-thick layer of sputtered IGZO. The Cu, Mo, and AZO layers were deposited as described above. The IGZO film was deposited by RF sputtering (Kenosistec KS 500C) at room temperature using a ceramic target with a composition In:Ga:Zn:O = 1:1:1:4. The deposition was done in a pure Ar environment with a flow rate of 10 sccm. No extra patterning step was performed as the sensors were directly realized through shadow masking approach.

4.3 | Electrical Characterization

The temperature response of the RTDs and thermistors were obtained using a multimeter (HP 34401A) to measure the resistance while the temperature was controlled using a hotplate. The initial assessment involved resistance measurement as a function of a single cycle of heating and cooling from 35°C to 115°C and vice versa. For this single cycle measurement, the hold time was 10 min at intervals of 10°C. Cycling measurement was conducted by real-time resistance measurement over five cycles of heating and cooling between 35°C and 95°C. At intervals of 20°C, the temperature was kept constant for 10 min.

4.4 | Mechanical Bending

The mechanical performance of the devices was evaluated by measuring the resistance of the sensors as a function of bending radius. The bending was performed by attaching the devices onto bending rods with defined bending radii from 25 mm down to 2.5 mm. The resistance was measured (Keithley 2636B SourceMeter) in flat, bent, and re-flat conditions.

4.5 | Life Cycle Assessment

Life cycle assessment (LCA) was applied in accordance with standards ISO 14040-14044 [37, 38]. The details of its constituting phases are given in the following subsections.

4.5.1 | Goal and Scope Definition

The aim of the present LCA study was to quantify the potential environmental impacts associated to the production of Mo-based RTDs on a TAC substrate and to compare them with those associated to the production of similar RTDs differing only in the employed substrate, the latter being constituted by a polyimide film. The functional unit selected was the production of a set (i.e., 1p) of Mo-based RTDs on a 7.5 cm × 7.5 cm substrate area. This set consists of 34 sensors with distinct geometry which cover a total area of 771 m^2 m. Besides the substrate fabrication, the boundaries of the studied system also included the cleaning of the substrate before deposition together with the sputtering of the molybdenum metal and the end of life of the waste materials generated. For the polyimide, a standard substrate preparation prior to any device fabrication is considered [9]: (1) 5 min in acetone with sonication, (2) 5 min in isopropanol with sonication, (3) baking at 200°C for 24 h. The experimentally demonstrated possibility to re-use the TAC substrate for a further device fabrication, after having removed Mo, was included to quantify the potential decrease into the associated environmental impacts.

4.5.2 | Life Cycle Inventory (LCI) and Life Cycle Impact Assessment (LCIA)

The life cycle inventories were modelled by employing datasets from the Ecoinvent database (version 3.10) by following an attributional approach, and specifically employing the APOS (i.e., allocation at the point of substitution) system model [39, 40]. The inventories were modeled in SimaPro 9.6.0.1 LCA software [41].

For the TAC substrate, since no dataset related to the production of TAC was available in Ecoinvent database, its inventory was modeled by considering a patented procedure [42] by the acetic acid process, the latter being the synthetic approach on which industrial TAC production mostly relies [43–46]. For the calculation of missing inventory data the model was complemented by the scale-up framework for chemical processes in LCA studies proposed by Piccinno et al. [47]. The complete inventories for the synthesis of TAC and the subsequent TAC substrate manufacturing are detailed in Tables S3, S4.

Concerning the Molybdenum deposition by sputtering, the original Ecoinvent (v. 3.10) dataset "Selective coat, copper sheet, sputter deposition {DE}— selective coating, copper sheet, and sputtering | APOS, U" was modified in order to replace Cr and Tin inputs by Mo, to replace German datasets with Italian ones and to account for the experimentally determined thickness of the Mo layer (i.e., 110 nm of pre-sputtering for target cleaning and 150 nm of effectively deposited Mo, for a total of 260 nm). The detailed inventory for Mo sputtering is reported in Table S5.

For the modeling of the conventional polyimide substrate, since no polyimide-specific datasets were available in Ecoinvent database, the environmental impact results (obtained with EF 3.1 method [35]) for high performance polyetherimide film [48] were employed. Those results were referred to the specific dataset named "High-performance film (polyetherimide) {EU-27}— technology-specific dataset (extension layer), polyetherimide resin conversion to high-performance film", an aggregated dataset from Carbonminds plastic database [49]. The use of the latter dataset as a proxy for the modelling of Kapton HN 200 (DuPont) was previously justified since both polymers feature aromatic backbones and imide linkages, thus showing similar rigidity and thermal stability [48]. Particularly, the environmental impacts reported in [48] and referred to 7 mg of high-performance polyetherimide film, were re- scaled to 1 kg and then used as the characterization factors (CFs) for a newly defined elementary flow (i.e., a newly defined non-material emission in SimaPro software named polyimide substrate), that was subsequently added to the EF 3.1 impact assessment method. The as calculated CFs of the newly defined polyimide elementary flow are detailed in Table S6. The LCI considered for the modeling of the polyimide substrate is detailed in Table S7.

Finally, the complete inventories for the modeling of the resistance temperature detectors fabricated on both TAC and polyimide substrates are detailed in Tables S8, S9.

In order to account for the experimentally demonstrated possibility to re-use the TAC substrate for the fabrication of further similar RTDs, the LCI of the RTDs fabricated on TAC substrate was modified to comprise for example the removal of Mo by employing deionized water, according to the details given in Table S10. Moreover, in order to account for the possibility to use the same amount of water for the concurrent cleaning of n sets of Mo-based RTDs on n substrates, the LCI (referred to one set of Mo-based RTDs on a TAC substrate employed for the fabrication of two devices) has been modified according to the details shown in Table S11.

The Life Cycle Impact Assessment (LCIA) phase was performed using the Environmental Footprint 3.1 (EF 3.1) method. This method was selected because it is a harmonized and scientifically robust framework developed within the European Environmental Footprint initiative, with methodological support from the European Commission's Joint Research Centre (JRC) [35]. The only modification to the EF 3.1 method was the above mentioned addition of the newly characterized (Table S4) polyimide non material emission, to account for the environmental footprint associated with the polyimide substrate production.

Acknowledgments

This work was supported by the Ministry of University and Research (Decree No. 22830 of December 5, 2024), Bando FIS 2, Project Title: Oxide-based thin-film devices upcycling for RecyclAble and CircuLar Electronics (ORACLE), CUP: E53C25000430001, Project Code: FIS-2023-02758, and in part by the Autonomous Province of Bozen-Bolzano through the International Joint Cooperation South Tyrol-Luxembourg SNF (V-SAFE), under Grant 7/34. The authors would like to thank Sabrina Wenke and Dr. Anne Pils of Island Polymer Industries GmbH for providing the TAC foils.

Conflicts of Interest

The authors declare no conflicts of interest.

Data Availability Statement

The data that support the findings of this study are available from the corresponding author upon reasonable request.

References

1. C. P. Baldé, R. Kuehr, T. Yamamoto, et al., "The Global E-Waste Monitor 2024," *International Telecommunication Union and United Nations Institute for Training and Research* (Griffith University, 2024).

2. G. A. Blengini, C. El Latunussa, U. Eynard, et al., *Study on the EU's List of Critical Raw Materials (2020) – Final Report* (Publications Office of the European Union, 2020).

3. N. Münzenrieder, L. Petti, G. A. Salvatore, and G. Cantarella, "Route Toward Sustainable Oxide TFTs: Does Thin Film Oxide Technology Offer a Pathway Toward More Sustainable Electronics?" *IEEE Electron Devices Magazine* 2, no. 2 (2024): 23–34.

4. J. H. Koo, D. C. Kim, H. J. Shim, T.-H. Kim, and D.-H. Kim, "Flexible and Stretchable Smart Display: Materials, Fabrication, Device Design, and System Integration," *Advanced Functional Materials* 28, no. 35 (2018): 1801834.

5. H. W. Choi, D.-W. Shin, J. Yang, et al., "Smart Textile Lighting/Display System with Multifunctional Fibre Devices for Large Scale Smart Home and IoT Applications," *Nature Communications* 13, no. 1 (2022): 814.

6. X. Shi, Y. Zuo, P. Zhai, et al., "Large-Area Display Textiles Integrated with Functional Systems," *Nature* 591, no. 7849 (2021): 240.

7. T. Y. Kim, J. W. Mok, S. H. Hong, et al., "Wireless Theranostic Smart Contact Lens for Monitoring and Control of Intraocular Pressure in Glaucoma," *Nature Communications* 13, no. 1 (2022): 6801.

8. L. E. Osborn, A. Dragomir, J. L. Betthauser, C. L. Hunt, H. H. Nguyen, R. R. Kaliki, and N. V. Thakor, "Prosthesis with Neuromorphic Multilayered E-Dermis Perceives Touch and Pain," *Science Robotics* 3, no. 19 (2018): eaat3818.

9. D. Corsino, F. Catania, K. Ishida, T. Meister, F. Ellinger, G. Cantarella, and N. Münzenrieder, "Monolithic Integration, Performance, and Comparison of Self-Aligned and Conventional IGZO Thin-Film Transistors on a Flexible Substrate," *IEEE Journal on Flexible Electronics* 1, no. 3 (2022): 159.

10. F. Catania, M. Ahmad, D. Corsino, N. Saeedzadeh Khaanghah, L. Petti, N. Münzenrieder, and G. Cantarella, "AC Performance of Flexible Transparent InGaZnO Thin-Film Transistors and Circuits," *IEEE Transactions on Electron Devices* 69, no. 9 (2022): 4930.

11. F. Le Goupil, G. Payrot, S. Khiev, W. Smaal, and G. Hadziioannou, "Fully Printed Sensors for In Situ Temperature, Heat Flow, and Thermal Conductivity Measurements in Flexible Devices," *ACS Omega* 8, no. 9 (2023): 8481.

12. Z. Skafi and T. M. Brown, *Conventional Substrates for Flexible Devices* (Springer Nature Switzerland, 2025), 27.

13. A. Rivadeneyra, M. Bobinger, A. Albrecht, M. Becherer, P. Lugli, A. Falco, and J. F. Salmerón, "Cost-Effective PEDOT:PSS Temperature Sensors Inkjetted on a Bendable Substrate by a Consumer Printer," *Polymers* 11, no. 5 (2019): 824.

14. K.-C. Ok, J.-H. Lim, H.-J. Jeong, H.-M. Lee, Y. S. Rim, and J.-S. Park, "Photothermally Activated Nanocrystalline Oxynitride with Superior Performance in Flexible Field-Effect Transistors," *ACS Applied Materials & Interfaces* 10, no. 3 (2018): 2709.

15. E. Toto, S. Laurenzi, R. C. Pellegrini, E. Cavallini, and M. G. Santonicola, "Eco-Friendly Synthesis of High-Performance Polyimide Materials Using Bio-Based Greener Solvents: Towards Sustainable Technologies in Space Environment," *Materials Today Sustainability* 25 (2024): 100657.

16. P. Sysel, H. Kulhánková, and K. Weinertová, "Polyimides Prepared Without the Use of Toxic Amidic Solvents," *Journal of Polymer Research* 27, no. 8 (2020): 227.

17. M. Djapovic, D. Milivojevic, T. Ilic-Tomic, et al., "Synthesis and Characterization of Polyethylene Terephthalate (PET) Precursors and Potential Degradation Products: Toxicity Study and Application in Discovery of Novel PETases," *Chemosphere* 275 (2021): 130005.

18. S. Li, H. Chen, X. Liu, P. Li, and W. Wu, "Nanocellulose as a Promising Substrate for Advanced Sensors and Their Applications," *International Journal of Biological Macromolecules* 218 (2022): 473.

19. F. Brunetti, A. Operamolla, S. Castro-Hermosa, G. Lucarelli, V. Manca, G. M. Farinola, and T. M. Brown, "Printed Solar Cells and Energy Storage Devices on Paper Substrates," *Advanced Functional Materials* 29, no. 21 (2019): 1806798.

20. M. Irimia-Vladu, E. D. Głowacki, G. Schwabegger, L. Leonat, H. Z. Akpinar, H. Sitter, S. Bauer, and N. S. Sariciftci, "Natural Resin Shellac as a Substrate and a Dielectric Layer for Organic Field-Effect Transistors," *Green Chemistry* 15 (2013): 1473.

21. G. Cantarella, M. Madagalam, I. Merino, et al., "Laser-Induced, Green and Biocompatible Paper-Based Devices for Circular Electronics," *Advanced Functional Materials* 33, no. 17 (2023): 2210422.

22. M. R. Radovanović, G. M. Stojanović, M. Simić, D. Suvara, L. Milić, S. Kojić, and B. D. Škrbić, "Edible Electronic Components Made from Recycled Food Waste," *Advanced Electronic Materials* 10, no. 7 (2024): 2300905.

23. Y. H. Jung, T.-H. Chang, H. Zhang, et al., "High-Performance Green Flexible Electronics Based on Biodegradable Cellulose Nanofibril Paper," *Nature Communications* 6, no. 1 (2015): 7170.

24. A. K. Jaiswal, V. Kumar, E. Jansson, et al., "Biodegradable Cellulose Nanocomposite Substrate for Recyclable Flexible Printed Electronics," *Advanced Electronic Materials* 9, no. 4 (2023): 2201094.

25. M. Qi, B. Liu, C. Chen, et al., "Ionic Liquid-Enabled Hydrogen-Bonding Networks in Corn Stalk-Derived Cellulose/Poly(Butylene Succinate) Composite Films for Sustainable Flexible Sensors," *International Journal of Biological Macromolecules* 353 (2026): 151187.

26. D. C. Corsino, M. Sait Abdusselamoglu, F. Catania, E. Avancini, N. Münzenrieder, and G. Cantarella, "Thin-Film Electronics on a Green and Flexible Cellulose-Based Film," *IEEE Transactions on Electron Devices* 71, no. 9 (2024): 5401.

27. V. U. Somkuwar, R. Pal, A. Layak, S. Hukkeri, and S. Periyasamy, "Silk-Based Materials for Sustainable Soft Electronics: Structure, Properties, and Emerging Applications," *The Journal of The Textile Institute* 117 (2026): 1126–1141.

28. L. Teuerle, T. Meier, K. Hänisch, et al., "Life-Cycle Assessment of Printed Electronic Components - Case Study for Organic Electrochemical Transistors," *Advanced Electronic Materials* 12 (2025): e00372.

29. T. Zhang, J. Harwell, J. Cameron, S. Zhang, H. Heidari, and J. Kettle, "Design for Recycling in Electronic Manufacturing: Enabling Circularity and Lower Impact Manufacturing Through Heterogeneous Integration and Lower Impact Recovery," *npj Materials Sustainability* 4, no. 1 (2026): 10.

30. Z. Song, Z. Chen, G. Du, et al., "Research Progress on Negative Temperature Coefficient Thermistors: Review," *Journal of Materials Science: Materials in Electronics* 36, no. 11 (2025): 688.

31. B. K. Ridley and T. B. Watkins, "The Possibility of Negative Resistance Effects in Semiconductors," *Proceedings of the Physical Society* 78, no. 2 (1961): 293.

32. A. Rasheed, S. Krik, S. Riaz, et al., "Thin-Film Thermal Sensors on Chitosan Substrates for Sustainable Transient Electronics," *Advanced Electronic Materials* (2026): e00699.

33. A. H. Lanthaler, S. Vasquez, R. Zamboni, et al., "IGZO-Based Thin-Film Thermistors on PEEK Fabric for Green Smart Textiles," *Advanced Electronic Materials* 11, no. 18 (2025): e00146.

34. N. Munzenrieder, C. Zysset, T. Kinkeldei, and G. Troster, "Design Rules for IGZO Logic Gates on Plastic Foil Enabling Operation at Bending Radii of 3.5 mm," *IEEE Transactions on Electron Devices* 59, no. 8 (2012): 2153.

35. S. Andreasi Bassi, F. Biganzoli, N. Ferrara, et al., "Updated Characterisation and Normalisation Factors for the Environmental Footprint 3.1 Method," *Publications Office of the European Union* (2023): KJ-NA-31-414-EN-N.

36. B. Bieda, "Application of Stochastic Approach Based on Monte Carlo (MC) Simulation for Life Cycle Inventory (LCI) to the Steel Process Chain: Case Study," *Science of the Total Environment* 481 (2013): 649.

37. International Organization for Standardization, "ISO 14040:2006, Environmental Management – Life Cycle Assessment – Principles and Framework," (International Organization for Standardization, 2006).

38. International Organization for Standardization, "ISO 14044:2006, Environmental Management – Life Cycle Assessment – Requirements and Guidelines," (International Organization for Standardization, 2006).

39. B. Weidema, C. Bauer, R. Hischier, et al., *Overview and Methodology: Data Quality Guideline for the Ecoinvent Database Version 3*, Ecoinvent Report No. 1 (Swiss Centre for Life Cycle Inventories, 2013).

40. G. Wernet, C. Bauer, B. Steubing, J. Reinhard, E. Moreno-Ruiz, and B. Weidema, "The Ecoinvent Database Version 3 (Part I): Overview and Methodology," *The International Journal of Life Cycle Assessment* 21, no. 9 (2016): 1218.

41. Pré Sustainability, "SimaPro 9.6.0.1," accessed February 12, 2024. Available, https://simapro.com.

42. C. J. Malm, "Precipitation of Cellulose Triacetate," U.S. Patent US 2,1800,009, November 1939. Available: https://patents.google.com/patent/US2180009A.

43. S. Fischer, K. Thümmler, B. Volkert, K. Hettrich, I. Schmidt, and K. Fischer, "Properties and Applications of Cellulose Acetate," *Macromolecular Symposia* 262, no. 1 (2008): 89.

44. H. Steinmeier, "3. Acetate Manufacturing, Process and Technology 3.1 Chemistry of Cellulose Acetylation," *Macromolecular Symposia* 208, no. 1 (2004): 49.

45. C. J. Malm, L. J. Tanghe, and B. C. Laird, "Preparation of Cellulose Acetate - Action of Sulfuric Acid," *Industrial & Engineering Chemistry* 38, no. 1 (1946): 77.

46. J. Wolfs and M. A. R. Meier, "A More Sustainable Synthesis Approach for Cellulose Acetate Using the DBU/CO2 Switchable Solvent System," *Green Chemistry* 23 (2021): 4410.

47. F. Piccinno, R. Hischier, S. Seeger, and C. Som, "From Laboratory to Industrial Scale: A Scale-Up Framework for Chemical Processes in Life Cycle Assessment Studies," *Journal of Cleaner Production* 135 (2016): 1085.

48. A. Costanzo, A. C. Bressi, M. Frey, F. Greco, and M. Niero, "Is Laser-Induced Graphene (LIG) Environmentally Sustainable? Laboratory-Scale Life Cycle Assessment of LIG from Petroleum- and Bio-Derived Precur-

sors," *The International Journal of Life Cycle Assessment* 30, no. 12 (2025): 3018.

49. "Carbon Footprint and LCA Data," Carbon Minds, accessed March 2026. Available, https://www.carbon-minds.com/products/data/carbon-footprint-and-lca-data/?nab=0.

Supporting Information

Additional supporting information can be found online in the Supporting Information section.

Supporting File: aelm70548-sup-0001-SuppMat.pdf.